Applied Catalysis B: Environmental 224 (2018) 264–275

Contents lists available at ScienceDirect

Applied Catalysis B: Environmental

journal homepage: www.elsevier.com/locate/apcatb

Research Paper

Novel V_2O_5-CeO_2-TiO_2-SO_4^{2-} nanostructured aerogel catalyst for the low temperature selective catalytic reduction of NO by NH_3 in excess O_2

Jihene Arfaoui[a,*], Abdelhamid Ghorbel[a], Carolina Petitto[b], Gerard Delahay[b]

[a] Université Tunis El Manar, Laboratoire de Chimie des Matériaux et Catalyse, Département de Chimie, Faculté des Sciences de Tunis, Campus Universitaire Farhat Hached d'El Manar, 2092, Tunis, Tunisia

[b] Institut Charles Gerhardt Montpellier, UMR 5253 CNRS/ENSCM/UM, Matériaux Avancés pour la Catalyse et la Santé, 8 rue de l'Ecole Normale, 34296 Montpellier Cedex 5, France

ARTICLE INFO

Dedicated to Professor Dr. Abdelhamid Ghorbel on the occasion of his 71th birthday

Keywords:
Nanostructured aerogel catalyst
V_2O_5-TiO_2
Ceria
Sulfate
NO-SCR by NH_3

ABSTRACT

New ceria and sulfate co-modified V_2O_5-TiO_2 aerogel catalysts were developed, using the one-step sol gel method associated with the supercritical drying process, for Diesel $DeNO_x$ technology. N_2 adsorption-desorption, XRD, H_2-TPR, NH_3-TPD, Raman and DRUV-Vis spectroscopy were employed to probe the physico-chemical properties of TiO_2, V_2O_5-TiO_2, V_2O_5-CeO_2-TiO_2 and V_2O_5-CeO_2-TiO_2-SO_4^{2-} aerogel materials. XPS was used to obtain further information about the oxidation states of the active sites on the surface of the novel V_2O_5-CeO_2-TiO_2-SO_4^{2-} aerogel catalyst. The characterization results showed the successful synthesis of a new generation of well nanostructured aerogel catalysts with high surface area, large porosity and good thermal stability. V, Ce and SO_4^{2-} actives species were found highly dispersed on TiO_2 surface and their presence strongly influenced the surface acidity and the redox properties of the aerogel catalysts. Sulfate anions created strong acid sites and most probably contributed to the stabilization of V and Ce surface species at their 4 + and 3 + oxidation state, respectively. In the SCR-NO by NH_3 under oxygen rich conditions, V_2O_5-TiO_2 aerogel catalyst exhibited low NO conversions in 150–500 °C temperature range. The addition of cerium significantly increased the NO conversion at low temperature (220–400 °C). However, the simultaneous incorporation of cerium and sulfate has led to a novel V_2O_5-CeO_2-TiO_2-SO_4^{2-} nanostructured aerogel catalyst with superior catalytic performances, at high temperature (450–500 °C), with respect to V_2O_5-WO_3/TiO_2 commercial one (EUROCAT).

1. Introduction

Nitrogen oxides (NO_x), emitted from the combustion of fuels in stationary and mobile sources, remain one of the major sources of air pollutants, that cause a variety of harmful environmental and human heath effects such as photochemical smog, acid rain, ozone depletion, fine particulate pollution, pneumonia, hay fever, bronchitis and cancer [1–4]. Selective catalytic reduction (SCR) with ammonia (NH_3) is regarded as the state-of-the-art technology for NO_x abatement. It was initially applied in the removal of NO_x from stationary sources and since 1970s, the commercially used catalysts are mainly WO_3 or MoO_3 doped V_2O_5/TiO_2 [5].

Over the last few years, the NH_3-SCR has also been introduced into the market for reducing NO_x emissions from mobile diesel engines (trucks or light vehicles) [6–8]. The three way catalysts (TWC) have been successfully used by the automotive industry for the simultaneously elimination of harmful emissions (NO_x, CO and unburned hydrocarbon (HC)) from gasoline-powered engines that work in stoechiometric air-to-fuel ratio. However, this system cannot be used for diesel vehicles, because of the oxygen-rich atmosphere where NO_x reduction cannot be easily achieved [8–10]. Hence, the removal of nitrogen oxides from diesel engine exhaust, under oxygen-rich conditions, remains one of the major challenges in environmental catalysis.

The reduction of NO_x emissions from diesel engine requires a highly efficient catalyst operating at high space velocity (GHSV) over a wide temperature range (200–500 °C) [11]. Great efforts have been devoted in heterogeneous catalysis to developing novel SCR catalyst with a good hydrothermal stability for real application in emission control from diesel engines. V_2O_5-WO_3(MoO_3)/TiO_2 is one of the commercial catalysts used for the NH_3-SCR process applied to diesel vehicles but there are still some drawbacks among them the high starting temperature, the narrow active temperature window (300–400 °C) and the low N_2 selectivity at high temperatures [12,13]. Iron and copper exchanged zeolites, especially ZSM-5, have also received much attention due to their superior NH_3-SCR activity under high GHSV. Nevertheless, the insufficient low-temperature activity of Fe-ZSM-5 and the poor

* Corresponding author.
E-mail address: jihenar@yahoo.fr (J. Arfaoui).

http://dx.doi.org/10.1016/j.apcatb.2017.10.059
Received 26 May 2017; Received in revised form 19 October 2017; Accepted 26 October 2017
Available online 28 October 2017
0926-3373/

hydrothermal stability of Cu-ZSM-5 are neither satisfactorily solved [13–15].

As revealed in the literature, the SCR process for mobile applications can be summarized by the followings main reaction [16]:

$4\ NH_3 + 4\ NO + O_2 \rightarrow 4\ N_2 + 6\ H_2O$ 1 (Standard SCR)

$2\ NH_3 + NO + NO_2 \rightarrow 2\ N_2 + 3\ H_2O$ 2 (Fast SCR)

$8\ NH_3 + 6\ NO_2 \rightarrow 7\ N_2 + 12\ H_2O$ 3 (NO_2-SCR)

Oxygen is indispensible for the standard NH_3-SCR through the oxidation of NO which is considered as the limiting step of the SCR reaction. The presence of NO_2, a stronger oxidant, in the reaction gases speeds up the reaction via the "fast SCR" pathway [17]. In practical conditions, O_2 is used in large excess, consequently the rate dependencies of the NO-SCR from oxygen have been neglected by many authors [12].

On commercial V_2O_5-WO_3/TiO_2 and metal-promoted zeolite catalysts, the standard SCR is the most important reaction: it proceeds between 250 °C and 450 °C in the presence of excess oxygen. However, the trend is now moving toward improving low-temperature performance through an increase of the NO_2/NO_x feed content: in fact, a 50% NO_2/NO_x ratio results in the fastest NO_x reduction [16].

Recently, much interest has been devoted to ceria based materials as a potential catalysts for the low-temperature NH_3-SCR due to the special fluorite structure of CeO_2 and its excellent redox properties [17,18]. This abundant, non-toxic and inexpensive compound, showed high oxygen storage capacity (OSC) with rapid formation and elimination of oxygen vacancies via the redox shift between Ce^{4+} and Ce^{3+} under oxidizing and reducing conditions, respectivelly [19,20]. It is well known that pure ceria is poorly thermostable and undergoes rapid sintering at high temperature thereby losing oxygen storage capacity [20,21]. To overcome this problem, cerium has often been used as an additive to enhance the activity of various catalysts for many applications such as: Photocatalysis [22,23], VOCs or CO oxidation [24–27] and NO removal [28–33]. In this framework, CeO_2/Fe-Ti-PILC [28], CeO_2/TiO_2 [21,29], Ce-W-Ti [15,30] and V_2O_5-CeO_2/TiO_2 [31,32] among other CeO_2 based catalysts have expressed high activity in selective catalytic reduction of NO by NH_3.

More recently, M. S. Maqbool et al. [33] have examined the sulfation effect on the low temperature NH_3-SCR activity of CeO_2 added Sb/V_2O_5/TiO_2, by SO_2 pretreatement of the catalyst under oxidizing conditions at different temperatures (300, 400 and 500 °C). The authors have concluded that SO_2 pretreatment at 500 °C has led to the maximum favorable sulfation with cerium (III) sulfate as the major surface species which were found more active in NO reduction than Ce(IV) sulfate formed by SO_2 pretreatment at 300 °C.

The promising role of sulfate has been also studied by W. Zhao et al. [34] who have reported several beneficial effects produced by S-doping V_2O_5/TiO_2 catalyst including: inhibition of rutile phase, increase of the surface area, enhancement of surface acidity, creation of oxygen vacancies and increase of active sites.

J. P. Chen et al. [35] have demonstrated that the number of acid sites increases when sulfur exists on the catalyst surface and this enhances NO removal activity by NH_3. On the other hand, R. Khodayari et al. [36] have reported that sulfating TiO_2/V_2O_5/WO_3 commercial SCR catalyst strengthened the active Brønsted acid sites which may increase and stabilize catalyst activity. Moreover, Z. Si et al. [37] have showed that sulfate groups improve the Brønsted acidity of CeO_2-ZrO_2-NiO-SO_4^{2-} catalyst leading to an increase of its high-temperature (> 300 °C) NH_3-SCR activity and N_2 selectivity.

Motivated by the attractive benefits of cerium supported species for their unique redox properties and sulfate anions for their beneficial acidic role, and taking into account that until now no studies concerning the direct co-modification of V_2O_5-TiO_2 catalyst by ceria and sulfate has been proposed for Diesel DeNOx technology, we have developed in this work, using the one step sol-gel method associated with the supercritical drying process, a new V_2O_5-CeO_2-TiO_2-SO_4^{2-} aerogel catalyst for the SCR-NO by NH_3 in a wide temperature range (150–500 °C), at relatively high GHSV (120.000 h^{-1}). The cerium was introduced with the aim of enhancing the NO-SCR activity at low temperature, while, sulfate groups were added in order to improve the N_2 selectivity at high temperature, through acidity. Therefore, the physicochemical characterizations, the study of both hydrothermal stability and resistance toward H_2O poisoning were devoted to the novel V_2O_5-CeO_2-TiO_2-SO_4^{2-} aerogel catalyst.

2. Experimental

2.1. Synthesis of TiO_2 support, V_2O_5-TiO_2, V_2O_5-CeO_2-TiO_2 and V_2O_5-CeO_2-TiO_2-SO_4^{2-} aerogel catalysts

Pure TiO_2 was synthesized via the one step sol-gel method (or single step sol-gel method [38]) using a similar procedure to that previously reported in reference [39] as follows: Ti(IV) isopropoxide ($Ti(O_iC_3H_7)_4$, Sigma-Aldrich, 97%), dissolved in anhydrous ethanol (C_2H_6O, Aldrich, 99.8%), was used as molecular precursor of TiO_2. In order to control the reaction kinetics, Ethyl acetoacetate ($C_6H_{10}O_3$, Fluka, > 99.5%) was used as a chemical additive (with a molar ratio Etacac/Ti = 1) to moderate the reaction rate. After aging under stirring at room temperature, a dilute solution of HNO_3 (0.1 M) was gradually added to accomplish hydrolysis according to the molar ratio H_2O/Ti = 10. The obtained homogenous gel was transformed into TiO_2 aerogel oxide, in autoclave, using the supercritical drying process of ethanol (T = 243 °C and P = 63 bar). The same procedure was used for the synthesis of V_2O_5-TiO_2, V_2O_5-CeO_2-TiO_2 and V_2O_5-CeO_2-TiO_2-SO_4^{2-} aerogel mixed oxides. Theoretical loading of ceria (10% wt.) or Vanadia (2% wt.) was introduced in the mixture by adding, under mechanical stirring and before hydrolysis, an appropriate amount of cerium nitrate ($Ce(NO_3)_3$. $6H_2O$, Aldrich, 99.5%) or vanadyl acetylacetonate ($V(C_5H_7O_2)_2$, Fluka, 95%). To obtain the sulfated catalyst, corresponding volume to S/Ti rate = 0.2 of H_2SO_4 solution (Scarlau, 95–97%) was added to the Ti-Ce-V organic mixture before the hydrolysis. All the aerogel mixed oxides were calcined for 3 h at 500 °C under O_2 flow (30 cc/min). The hydrothermal treatment was done in order to estimate the resistance of V_2O_5-CeO_2-TiO_2 containing sulfates only. For this, we have chosen a hydrotreatment in dynamic with a final temperature of 625 °C and a time of 16 h under 10% H_2O/air: hydrothermal treatment very close to that used by Marberger et al. [40] for their NH_3-SCR study over V_2O_5/WO_3-TiO_2 catalysts. The hydrothermal aged catalyst is denoted as V_2O_5-CeO_2-TiO_2-SO_4^{2-} HT.

2.2. Characterization of the TiO_2 support and the mixed oxides aerogel catalysts

2.2.1. N_2 adsorption-desorption at 77 K

Textural properties of the aerogel materials were determined by N_2 adsorption/desorption at 77 K using a Micromeritics ASAP 2020 apparatus. The samples were outgassed in a vacuum during 6 h at 200 °C prior to analysis.

2.2.2. X-ray diffraction (XRD)

The crystal phases of the solids were identified by X-ray powder diffraction using a Brüker AXS D8 diffractometer with CuKα radiation (λ = 1.5406 Å). The scanning range was collected from 2θ = 2° to 80° with a step size of 0.02°. The crystallite size (D) of TiO_2 was estimated from the characteristic peak around 2θ = 25° for the (101) reflection of anatase phase by using the Scherrer formula [41]:

$$D = 0.89\ (\lambda/\beta\cos\theta)$$

Where, λ is the wavelength of XR radiation, β is the corrected peak

width at half-maximum intensity (FWHM in radians), and θ is the peak position of the main reflection.

2.2.3. Raman spectroscopy

Raman measurements were performed at room temperature in backscattering configuration using a T64000 Jobin-Yvon Spectrometer. The light excitation is provided by the 488 nm line of an Ar^+ laser. The incident power is taken equal to 5 mW at sample surface.

2.2.4. X-ray photoelectron spectroscopy

XPS analysis were realized with the device ESCALAB 250 of thermo electron with a monochromatic ray Al Kα (1486.6 eV) as the excitation source. The analyzed surface has a diameter of 400 μm and the X-ray Photoelectron spectra are calibrated in binding energy with regard to the binding energy of the C—C bond of the carbon C1 s at 284.8 eV. The charge is compensated with an electron beam (−2 eV).

2.2.5. DRUV-Vis spectroscopy

UV–vis diffuse reflectances were recorded on a PerkinElmer spectrophotometer type instrument lambda 45 coupled to an integration sphere type RSA-PE-20 in the range of 200–900 nm with a speed of 960 nm min^{-1} and an aperture of 4 nm.

2.2.6. Temperature programmed reduction of H_2 (H_2-TPR)

Temperature programmed reduction have been carried out in a quartz fixed-bed micro-reactor using an AUTOCHEM 2920 (Micromeritics) equipped with a TCD detector. Prior to H_2-TPR measurements, the catalyst (0.05 g) was pre-treated under 5 vol% O_2 in He (flow rate = 30 mL min^{-1}) at 500 °C (ramp 10 °C min^{-1}) for 30 min. After being cooled down to 50 °C in the same atmosphere, the sample was flushed with He (30 mL min^{-1}) then exposed to a flow containing 5 vol% H_2 in Ar (30 mL min^{-1}) and heated between 50 °C and 800 °C with a heating rate of 10 °C min^{-1}.

2.2.7. Temperature programmed desorption of ammonia (NH_3-TPD)

Total acidity of the catalysts was evaluated by a temperature-programmed desorption (TPD) of ammonia using an AUTOCHEM 2910 (Micromeritics). Before NH_3 adsorption, the samples were pre-treated under air flow (30 mL min^{-1}) at 500 °C (ramp 10 °C min^{-1}) for 30 min. NH_3 adsorption was done at 100 °C using 5 vol% NH_3 in He (flow rate = 30 mL min^{-1}) for 45 min and then flushed with He (30 mL min^{-1}) during 2 h to remove physisorbed NH_3. Finally, the ammonia was desorbed in helium flow (30 mL min^{-1}) from 100 °C to 600 °C using a heating rate of 10 °C min^{-1}.

2.3. Catalytic test

The selective catalytic reduction (SCR) of NO by NH_3 was carried out in a fixed-bed quartz flow reactor operating at atmospheric pressure. The catalyst (0.05 g) was activated in situ at 200 °C for 30 min under O_2/He (20/80, v/v) flow then cooled to 150 °C. A feed gas stream, containing 400 ppm NO, 400 ppm NH_3 and 8% O_2 in He as a balance gas, was supplied through mass flow controllers to the micro-reactor with a total flow rate of 100 cm^3 min^{-1} yielding a gas hourly space velocity (GHSV) of 120,000 h^{-1}. The SCR was carried out on programmed temperature from 150 to 500 °C with the heating rate 6 °C min^{-1}. The reactants and products were analyzed by a quadruple mass spectrometer (Pfeiffer Omnistar) equipped with Channeltron and Faraday detectors (0–200 amu).

3. Results and discussions

3.1. N_2-Adsorption-desorption at 77 K

Textural properties of the samples, including specific surface area (S_{BET}), BJH desorption pore volume (V_{PT}) and pore size diameter

Table 1
Textural properties of TiO_2 support and the aerogel catalysts.

Sample	BET surface area (m^2/g)	Total pore volume (cm^3/g)	Average Pore diameter (Φ_{pore}, Å)
TiO_2	122	0.33	79
V_2O_5-TiO_2	101	0.37	117
V_2O_5-CeO_2-TiO_2	82	0.33	133
V_2O_5-CeO_2-TiO_2-SO_4^{2-}	66	0.26	157
V_2O_5-CeO_2-TiO_2-SO_4^{2-} HT	51	0.31	249

(Φ_{pore}) are summarized in Table 1. As it can be noticed, the aerogel TiO_2 is classified as mesoporous material with an average pore diameter of 79 Å and exhibits, after calcination at 500 °C, higher surface area (122 m^2/g) compared to that characterizing the commercial TiO_2 Degussa P25 (~50 m^2/g) [42]. This result is in perfect agreement with that previously obtained by C. Gannoun et al. [39] and obviously shows the advantage of the use of the sol gel method associated with the supercritical drying process for the synthesis of mesoporous materials having high surface area and large porosity. After cerium, vanadium and sulfate addition onto TiO_2 support and after the hydrotreatment of V_2O_5-CeO_2-TiO_2-SO_4^{2-} at 625 °C, the surface area decreases but remains above 50 m^2/g. The loss of the surface area can be explained by the blocking of some pores of the support by the deposited active species as already suggested for various metal supported catalysts [43–45].

N_2 adsorption-desorption isotherms at 77 K and pore size distribution curves of the aerogel materials are displayed in Figs. 1 and 2, respectively. According to the IUPAC classification [46], all the samples are characterized by the type IV isotherms (behavior characteristic of mesoporous materials) with hysteresis loops type H2 or H1: H2 type, registered in the case of TiO_2 support, indicates the existence of an inkbottle-type pores structure with narrow necks and wide bodies [46,47], while H1 type, observed for all the aerogel catalysts, is often associated with porous materials known to consist of agglomerates or compacts of approximately uniform spheres in fairly regular array [46].

It is clearly seen from the pore size distribution curves of the samples (Fig. 2) that the modification of TiO_2 by Ce, V and SO_4^{2-} contributes to the enlargement of its pores probably due to the strong interactions between the active species and the support. A similar effect is observed after the hydrothermal aging of V_2O_5-CeO_2-TiO_2-SO_4^{2-} catalyst at 625 °C.

3.2. X-ray diffraction

Fig. 3 shows the XRD patterns of the aerogel samples. Only the typical reflections of the anatase phase at 2θ = 25.3° (*hkl*:101); 36.9°

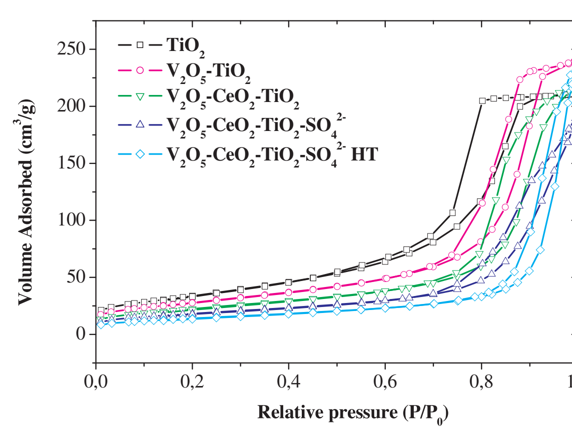

Fig. 1. N_2 Adsorption-desorption isotherms of the nanostructured aerogel catalysts.

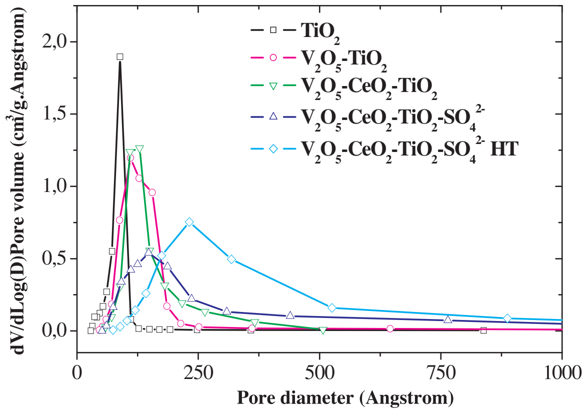

Fig. 2. Pore size distribution curves of the nanostructured aerogel catalysts.

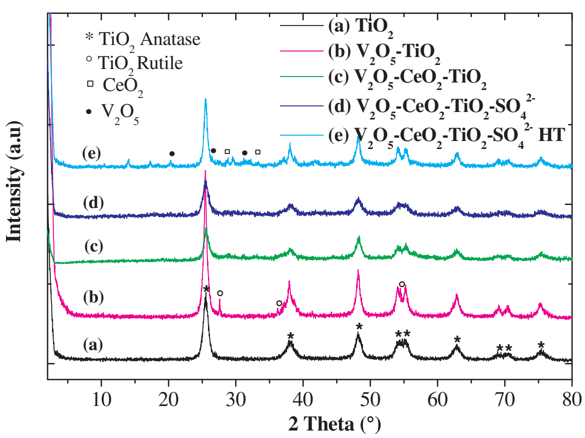

Fig. 3. XRD patterns of the nanostructured aerogel catalysts.

(103); 37.8° (004); 38.6° (112); 48.2° (200); 53.9° (105); 55.2° (211); 62.7° (204); 69.0° (116); 70.4° (220) and 75.2° (215) [ICSD 01-083-2243] are detected on the diffractogram of TiO_2 aerogel support. This observation is different from that previously reported by X. Gao et al. [21] who have demonstrated the formation of anatase, rutile and brookite phases in the xerogel TiO_2, classically dried at 80 °C. This underlines the key role of the supercritical drying process in the preparation of a well nano-structured TiO_2 derived sol gel anatase phase with higher purity (100%) with respect to the commercial TiO_2 Degussa P25 which is a mixture of 75% anatase and 25% rutile [42]. It is known that TiO_2 with mainly anatase phase exhibits better catalytic activity compared to TiO_2 with mixed anatase and rutile phases [48].

According to the strong anatase (101) diffraction peak (around 2θ = 25°), the average crystallite size of the aerogel samples was calculated and given in Table 2. It can be concluded that the crystallite size of the well structured TiO_2 anatase phase is slightly affected by the nature of the deposited active species and ranges from ~8 to ~13 nm. This proves the success synthesis of a highly structured aerogel materials with nanometer size as catalysts for the NH_3-SCR process. Generally, smaller crystallite size of the catalyst yields a large surface area which promotes the dispersion degree of the active components and consequently enhances the catalytic performances [34].

It should be mentioned that no reflections associated with CeO_2; Ce_2O_3; VO_2 and V_2O_5 crystalline phases, principally identified at 2θ = 28.5° (111) [PDF 00-034-0394]; 2θ = 30.4° (011) [ICSD 01-074-1145]; 2θ = 27.7° (110) [ICSD 01-079-1655] and 2θ = 20.2° (001) [ICSD 01-089-2482], respectively, are found for all the catalysts calcined at 500 °C revealing that V and Ce exist in the form of highly dispersed surface species [34,49]. On the other hand, no diffraction peaks belonging to the tetragonal phase of $CeVO_4$ (most intense one at 2θ = 24° (200) [50]) are observed for the samples containing both cerium and vanadium. In addition, none of the possible cerium sulfate species; $Ce(SO_4)_2$ (major peak at 2θ = 19.1° (112) [ICSD 01-070-2097]) and $Ce_2(SO_4)_3$ (major peaks at 2θ = 16,1° and 31,3° [PDF 00-001-0208]), are detected on the sulfated catalyst calcined at 500 °C.

It is worth mentioning that the weak peaks observed at 2θ = 27.2° (110), 35.7° (101) and 53.9° (211) in the diffractogram of V_2O_5-TiO_2 catalyst are attributed to a trace amount of rutile phase [ICSD 01-076-1941], while, the peaks of very low intensity which have appeared at 2θ = 20.2°, 26.3°, 31.2° and at 2θ = 28.5°, 33.2°, after the hydrothermal aging of V_2O_5-CeO_2-TiO_2-SO_4^2 at 625 °C, can be ascribed to a very low quantity of V_2O_5 and CeO_2 crystalline phases, respectively. The formation of these oxides, in a trace amount, with the quasi-preservation of the crystalline structure of the TiO_2 anatase phase without any rutilization (Usually occurs between 500 and 600 °C [51]) may serve as a proof for the high thermal stability of V_2O_5-CeO_2-TiO_2-SO_4^{2-} hydrothermal aged catalyst.

It seems also that, during the hydrothermal aging of V_2O_5-CeO_2-TiO_2-SO_4^{2-} sample, Ce species interact with SO_4^{2-} anions to form $Ce_2(SO_4)_3$ compound which is probably identified by the low intensity peaks detected around 2θ = 14°, 18.2°, 29.5° and 31.3° on the diffractogram of V_2O_5-CeO_2-TiO_2-SO_4^{2-} HT.

Table 2
XRD phases and TiO_2 crystallite size of the aerogel catalysts.

Sample	XRD phases	FWHM (°)	TiO_2 crystallite size D (nm)
TiO_2	Anatase	0.8920	8.66
V_2O_5-TiO_2	Anatase + Rutile (*t)	0.6259	12.41
V_2O_5-CeO_2-TiO_2	Anatase	0.7615	10.20
V_2O_5-CeO_2-TiO_2-SO_4^{2-}	Anatase	0.9900	7.80
V_2O_5-CeO_2-TiO_2-SO_4^{2-}HT	Anatase + V_2O_5 (t) + CeO_2 (t)	0.5850	13.22

With **t* = *trace amount*.

3.3. Raman spectroscopy

Raman spectra of the aerogel catalysts are presented in Fig. 4. The bands at 145, 197, 396, 515 and 637 cm^{-1} are observed for all the samples and could be assigned to E_g, E_g, B_{1g}, A_{1g} and E_g modes of TiO_2 anatase phase, respectively [23,41,52]. The strong and the medium peaks at 145 and 637 cm^{-1} are ascribed to the bending vibrations and symmetrical stretching vibrations of O-Ti-O, respectively [41]. Whereas, the weak peaks at 396 and 515 cm^{-1} correspond to the symmetric and unsymmetrical bending vibrations of O-Ti-O, respectively [41]. No typical Raman bands belonging to the crystalline phases

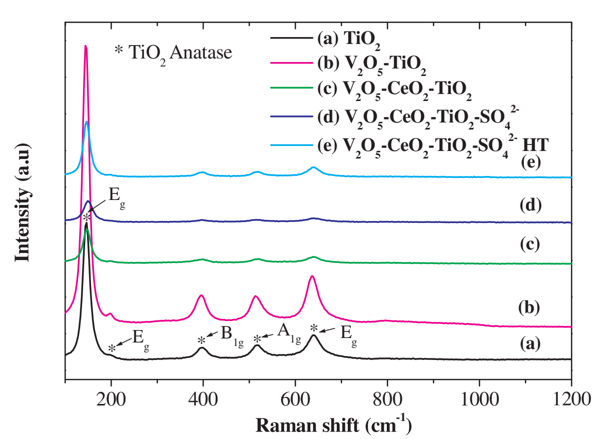

Fig. 4. Raman spectra of the nanostructured aerogel catalysts.

of CeO_2 (F_{2g} mode of O-Ce-O vibrations around 465 cm^{-1} [23,41,52]), V_2O_5 (994 cm^{-1} [53,54]) and $CeVO_4$ (850 cm^{-1} [52,54]) are detected for all the catalysts calcined at 500 °C suggesting, in line with the XRD results, the highly dispersed state of vanadium and cerium on the catalysts surface.

In spite of the fact that the XRD pattern of V_2O_5-CeO_2-TiO_2-SO_4^{2-} HT exhibits very weak peaks ascribable to CeO_2 and V_2O_5 crystalline phases, its Raman spectrum did not show any sign for the presence of these oxides. Similar observations have been previously reported by X. Gu et al. [54] and C. Gannoun et al. [24].

The characteristic bands of the well dispersed VO_x species on the TiO_2 support, generally observed in 800–1050 cm^{-1} range [52], and those related to the sulfate anions, usually detected around 994, 1360 and 1168 cm^{-1} [44], are not found in the case of our samples. This may be due to the low loading of vanadium and sulfates as explained earlier [24,32].

3.4. X-ray photoelectron spectroscopy

The oxidation states of V and Ce on the surface of VTi and VCeTi catalysts have been extensively studied using XPS and most of the authors agree that V^{5+}/V^{4+} and Ce^{4+}/Ce^{3+} forms exist on the catalysts surface [24,39,55]. In this study, the XPS analysis was devoted to the novel V_2O_5-CeO_2-TiO_2-SO_4^{2-} to get an idea about the nature of the active sites present on its surface. The XPS results of Ti, O, Ce, V and S are illustrated in Fig. 5.

The XPS result of Ti 2p (Fig. 5 a) shows two peaks centered at 459.0 and 464.9 eV. These binding energy (Ti 2p3/2 and Ti 2p1/2), corresponding to the typical Ti^{4+} oxidation state in a tetragonal structure [56], appear at higher values compared to those usually observed for pure TiO_2 (458.1 and 463.8 eV) [57]. This is a clear indication about the existence of strong interactions between V, Ce and/or SO_4^{2-} supported species and TiO_2 support [56,57]. The interaction between sulfate anion and titanium cation is believed to be a driving force for the generation of large amount of surface acid sites on sulfated metal oxides [58].

Two peaks are detected in the XPS spectra of O1 s (Fig. 5b): the peak at lower binding energy (centered at 530.2 eV) could be attributed to the lattice oxygen O^{2-} (denoted as Oβ) [11] and the peak at higher binding energy (centered at 531.8 eV) can be assigned to several O1 s states of surface adsorbed oxygen (denoted as Oα) such as O_2^{2-} or O^- belonging to defect oxide or hydroxyl like group, and chemisorbed water [11,56,59]. Many researchers considered that surface adsorbed oxygen (Oα) is more reactive than lattice oxygen (Oβ) in the oxidation reaction due to its higher mobility [11,59], consequently Oα is beneficial for the NO oxidation to NO_2 in the SCR reaction and it enhances the $DeNO_x$ efficiency at low temperatures [60].

Complicated XPS spectra of Ce 3d is displayed in Fig. 5c. The most intense and clearly seen peaks with binding energies of 904.8 and 886.2 eV represent $3d^{10}4f^1$ initial electronic state of Ce^{3+} [11,56], whereas, the satellite peak observed at 917.8 eV correspond to $3d^{10}4f^0$ state of Ce^{4+} [11,56]. This result demonstrates, in perfect agreement with several previous investigations [24,33,61,62], the predominance of Ce^{3+} form on the surface of the sulfated catalyst. In a previous work of our group, C. Gannoun *et al.* [24] have observed cerium at both 3+ and 4+ oxidation states on VTiCe catalyst surface but they have detected only Ce^{3+} on the surface of the same sulfated catalyst (VCeTiS). Similarly, M. S Maqbool et al. [33] and S. Gao et al. [61] have demonstrated a Ce^{3+} surface enrichment after sulfation of CeO_2-Sb-V_2O_5/TiO_2 and CeZ catalysts, respectively. Furthermore, X-s Du et al. [62] have observed a Ce^{4+} to Ce^{3+} transformation during the pre-sulfation of Ce-Ti oxide catalyst. Accordingly, the high capacity of V_2O_5-CeO_2-TiO_2-SO_4^{2-} to stabilize Ce^{3+} ions can reveal the existence of a strong interactions between cerium species and sulfate groups.

Only one intense peak centered at 515.6 eV is detected in the XPS spectra of V 2p3/2 (Fig. 5 d) and is assigned to V^{4+} surface species [55]. A weak shoulder can be localized around 517.3 eV and can be ascribed to a very low amount of V^{5+} on the surface of V_2O_5-CeO_2-TiO_2-SO_4^{2-} aerogel mixed oxides [55]. This result, indicating that vanadium mainly exist in V^{4+} form, agrees with the result already obtained by W. Zhao *et al.* [34] reporting an increase of $V^{4+}/(V^{4+} + V^{5+})$ atomic ratio by S doping V_2O_5-TiO_2 catalyst. Thus, we can suggest the existence of strong interactions between vanadium species and sulfate anions which probably contribute to stabilize vanadium at its 4 + oxidation state.

The peak situated at 169.0 eV in the S 2p binding energy region (Fig. 5 e) is related to the sulfur in its highest oxidation state (VI) in the $-SO_4^{2-}$ species [57]. The absence of peaks at 161-162.8 eV and 164 eV attributable to sulfide and elemental sulfur, respectively, [58,63,64] implies that S^{6+} might be present in the form of bidentately coordinated SO_4^{2-} on the surface of TiO_2 either chelating or bridging, as proposed in the literature [58,63,64].

3.5. DR UV–vis spectroscopy

The UV–vis diffuse-reflectance spectroscopy can provide the information about different oxidation states and local coordination state of titanium, vanadium and cerium species in the solid. Generally, two kinds of transitions can be measured in the UV–vis spectrum of transition metals: d–d and ligand-to-metal charge transfer (LMCT) transitions. The energy of d–d transitions depends on the metal oxidation state, however the one of charge transfer transitions is influenced by both the local coordination environment and the polymerization.

DR UV–vis spectra of the aerogel catalysts are illustrated in Fig. 6. The TiO_2 support shows a typical absorption band in 200–400 nm range with four absorption maximum attributable to tetrahedrally coordinated Ti^{4+} (217 nm), octahedrally coordinated Ti^{4+} (275 nm) and anatase crystal form (320 and 350 nm) [65,66]. The new peaks observed in 350–400 nm range for the catalysts containing vanadium, having a higher intensity in the case of the unsulfated samples, are assigned to $O^{2-} \rightarrow V^{5+}$ charge transfer (CT) transitions in different surface VO_x species [65–67]. The value of these electronic CT energies are strongly influenced by the local structure of V sites (the number of oxygen atoms surrounding the central V^{5+}) and the size of the V domains investigated. Higher coordination number and higher degree of polymerization generally result in a shift of the charge transfer transition to lower energy (higher wavelength) [67,68]. Hence, the first absorption band centered around 357 nm corresponds to oligomeric tetrahedral VO_x chains [69], whereas, the second one located around 390 nm indicates the presence of low polymeric tetrahedral VO_x chains [65] or V in square pyramidal configuration [65–67]. The oligomeric and polymeric VO_x chains are formed by the condensation of the monomeric tetrahedral vanadium species with the formation of V—O—V bridges.

Based on the literature, highly dispersed monomeric tetrahedral V^{4+} and V^{5+} species are identified by oxygen → vanadium CT bands in the range of 240–280 nm and 280–340 nm, respectively [70]. While, cerium species are characterized by $O^{2-} \rightarrow Ce^{n+}$ CT transitions around 220 and 250 nm for tetracoordinated Ce^{3+} [71,72] and in the range of 280–300 nm for tetracoordinated Ce^{4+} [71,72]. However, the position of ($O^{2-} \rightarrow Ce^{4+}$) band depends on the ligand field symmetry surrounding the Ce center. The electronic transitions require higher energy for tetracoordinated Ce^{4+} (~300 nm) than for hexacoordinated one (~400 nm) [73].

A substantial increase in the intensity of the bands situated around 220 nm and in 240–280 nm range, accompanied by a notable decrease in the intensity of those located around 400 nm are observed in the V_2O_5-CeO_2-TiO_2-SO_4^{2-} spectrum (Fig. 6). These observations may indicate a Ce^{3+} and V^{4+} enrichment of the sulfated catalyst surface and could demonstrate, in line with the XPS results, a high capacity of the sulfate anions to stabilize cerium and vanadium species at their 3+ and 4+ oxidation state, respectively. Similar conclusions have been already

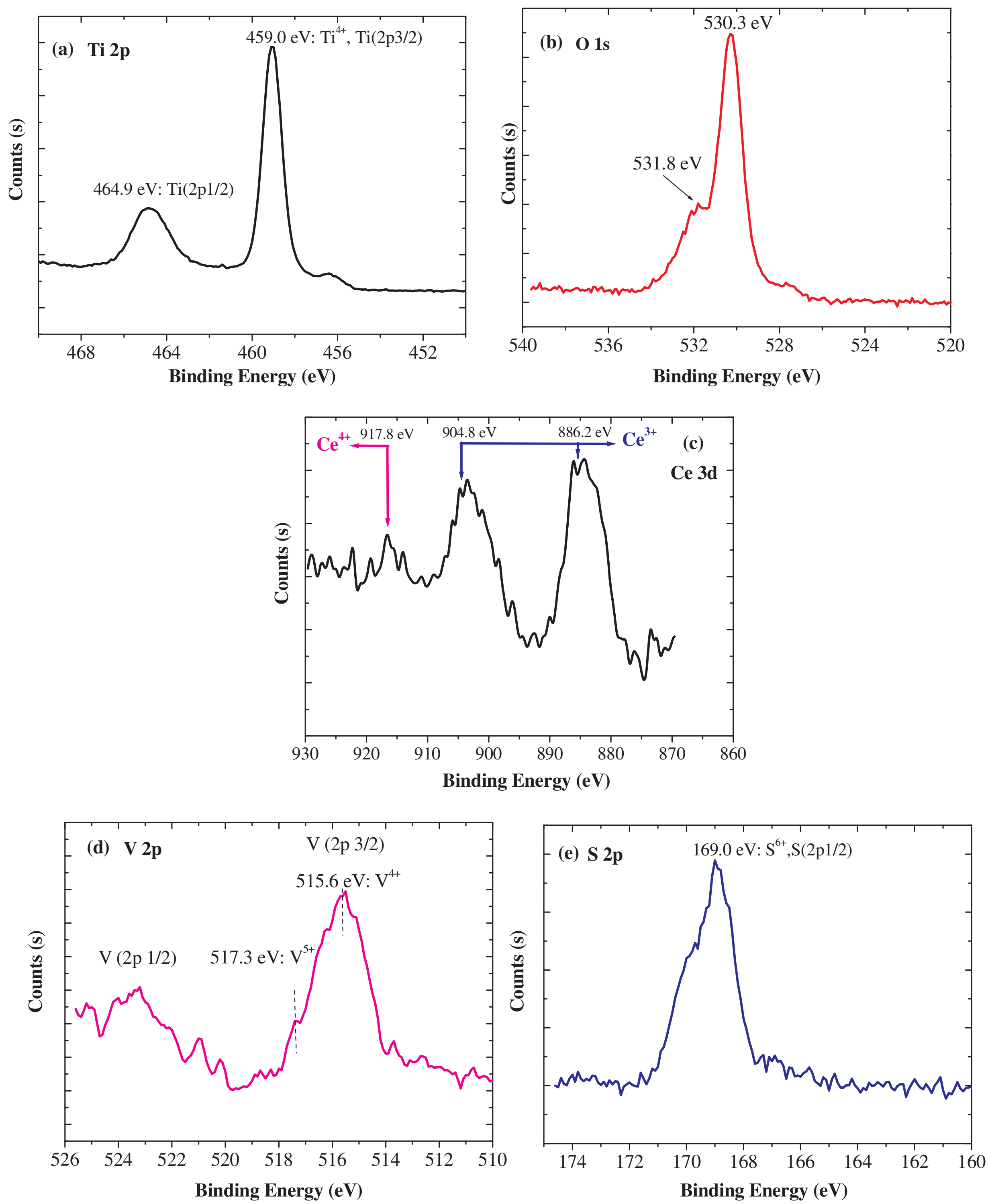

Fig. 5. XPS results over the novel V_2O_5-CeO_2-TiO_2-SO_4^{2-} nanostructured aerogel catalyst.

reported by S. Gao et al. [61] for ceria supported on sulfated zirconia system (CeSZ) and by L. Baraket et al. [63] for VSTi catalyst.

After hydrotreatment of V_2O_5-CeO_2-TiO_2-SO_4^{2-} at 625 °C, a broad band maximizing around 300 nm is observed and it can be essentially related to oxygen → metal CT transitions of monomeric tetra-coordinated V^{5+} and Ce^{4+} species. Their predominance in the V_2O_5-CeO_2-TiO_2-SO_4^{2-} HT system seems to be favored by the sulfate departure during the hydrothermal aging of the sample at 625 °C for 16 h. This is consistent with the result previously obtained by Z. Li et al. [11] demonstrating the formation of more Ce^{4+} on the surface of Ce-W/Ti catalyst after the hydrothermal treatment of the solid at 670 °C (5% H_2O/air for 64 h).

Noting that the weak absorption bands observed around 520 nm and 665 nm for all the samples can be assigned to a low amount of cristalline V_2O_5, probably too small to be detected by XRD technique, and to V^{4+} d–d transitions, respectively [74].

3.6. H_2-TPR

The reducibility of catalysts is a crucial feature for the NO-SCR

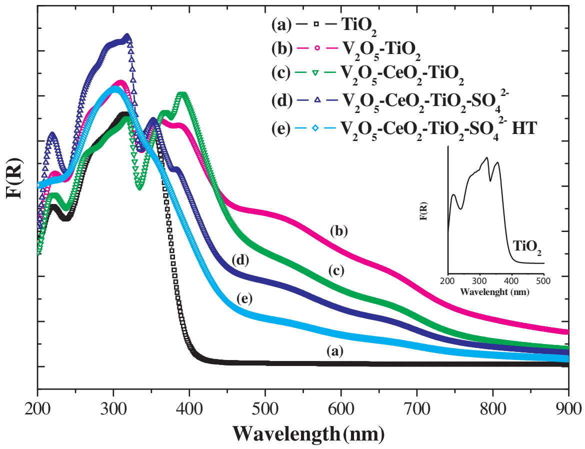

Fig. 6. DRUV-Vis spectra of the nanostructured aerogel catalysts.

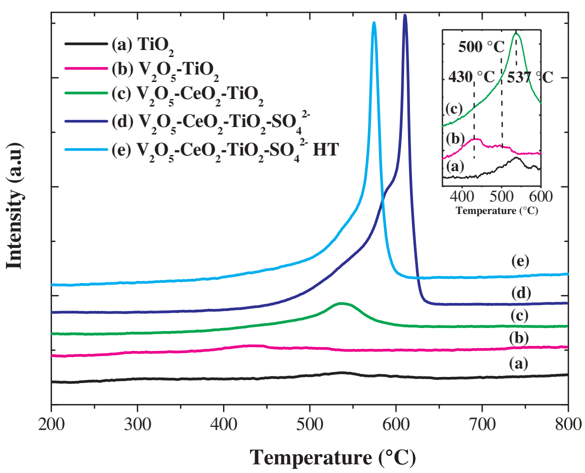

Fig. 7. H_2-TPR profiles of the nanostructured aerogel catalysts.

reaction. H_2-TPR analysis was carried out to investigate the redox properties of the aerogel oxides and the obtained H_2-TPR profiles are presented in Fig. 7. In contrary to a previous report that several peaks above 650 °C were obtained for bulk V_2O_5 [75], only two unresolved peaks maximizing at 430 °C and 500 °C are detected for V_2O_5-TiO_2 sample and can be assigned to the reduction of highly dispersed VO_x species [11]. After ceria addition, a new peak centered at 537 °C is appeared in the TPR profile of the binary V_2O_5-CeO_2-TiO_2 and can be attributed to the reduction of surface Ce^{4+} to Ce^{3+} [24,54]. For the ternary V_2O_5-CeO_2-TiO_2-SO_4^{2-}, a twin peaks relating to the reduction of different types of sulfate species (SO_4^{2-}) conforming to different sulfate structures are detected at 593 and 610 °C [24,63,76–78]. It seems that the sulfate anions not strongly bonded to the surface (probably those interacting only with the supported species) are reduced at lower temperature than those strongly interacting with the surface (possibly those interacting with both the TiO_2 support and the supported species).

After the hydrotreatment of V_2O_5-CeO_2-TiO_2-SO_4^{2-} catalyst, the first peak related to sulfate reduction was disappeared and the second one was moved to lower temperature (from 610 °C to 574 °C). This could indicate a departure of sulfate groups not strongly bonded to the surface and a more easily reduction of sulfate anions strongly bonded to the surface. It can be concluded that the long time hydrothermal aging weakens the interaction between sulfate and other atoms.

A slight decrease in the intensity of the peaks related to V and Ce reduction is observed in the TPR profile of V_2O_5-CeO_2-TiO_2-SO_4^{2-} HT sample and can be correlated, based on the XRD results, with the crystallization of a small amounts of CeO_2 and V_2O_5.

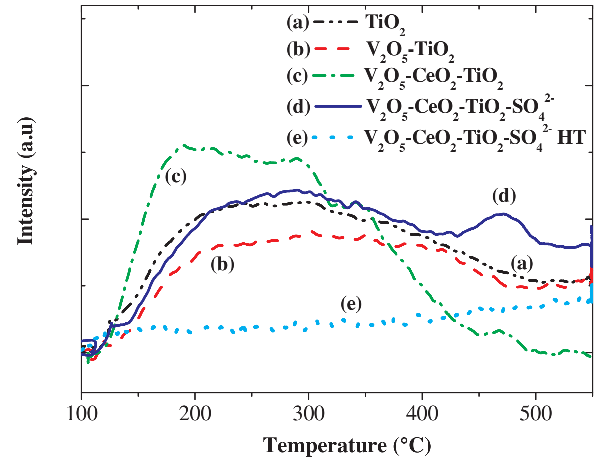

Fig. 8. NH_3-TPD profiles of the nanostructured aerogel catalysts.

3.7. NH_3-TPD

It is well known that ammonia (NH_3) is an excellent probe molecule for testing the acidic properties of solids as its strong basicity and small molecular size allow the detection of acid sites located also into very narrow pores. This molecule can be adsorbed on Brønsted and Lewis acid sites to form NH_4^+ and coordinated NH_3 in the NO-SCR reaction. Therefore, the surface acidity of the catalyst is critical for this reaction.

According to the literature, NH_3-desorption peaks with maximum in the range of 180–250 °C, 260–330 °C, 340–500 °C are currently attributed to NH_3 chemisorbed on weak, medium and strong acid sites, respectively [79]. The strength of acid sites present on the catalysts surface were determined by TPD of ammonia and the NH_3-desorption curves from 100 to 550 °C are displayed in Fig. 8. All the catalysts calcined at 500 °C show two broad peaks: the first one, located in 100–250 °C temperature range, is attributed to ammonia desorption from weak acid sites and the second one, situated in 250–450 °C range, corresponds to desorbed ammonia from medium strong acid sites. Beside these broad peaks, a new well resolved peak centered around 470 °C is appeared in the NH_3-TPD profile of the sulfated sample indicating that sulfate groups generate a new type of strong acid sites on the surface of V_2O_5-CeO_2-TiO_2-SO_4^{2-} catalyst and consequently improve its total acidity. This result agrees with most reports existing in the literature, demonstrating that catalysts with metal sulfates, such as TiO_2-SO_4^{2-} [80], V_2O_5-TiO_2-SO_4^{2-} [24,64], VSTi-PILC [81], CeO_2-SO_4^{2-} [82], VTiS, VCeS, VZrS and VAlS [77], can generated large amounts of acid sites on the surface. It was proposed that sulfate species interact with adsorbed water to form Brønsted acid sites promoting the adsorption of ammonia and consequently facilitating the NH_3-SCR reaction [83]. Moreover, X. Guo et al. [84] have claimed that an excellent NO reduction activity was observed since the density of Brønsted acid sites was increased upon sulfation of V_2O_5/TiO_2 system.

The hydrothermal treatment dramatically decreases the total acidity of V_2O_5-CeO_2-TiO_2-SO_4^{2-} HT which is in perfect agreement with several reported literature studies [85,86]. The loss of the surface acidity during the hydrothermal aging of the catalyst is most probably due to the sulfate departure, as evidenced by H_2-TPR analysis, and to a likely modification of the interactions between different atoms (Ti, Ce, V and SO_4^{2-}) which inhibits the NH_3 adsorption.

3.8. Catalytic test

According to the most accepted NH_3-SCR mechanisms (Eley-Rideal and Langmuir-Hinshelwood mechanisms), two factors play a very important role in $DeNO_x$ reaction: acidity and redox properties of the catalyst [12,87]. Lietti et al. [88] reported that the catalyst redox functions govern the catalytic reactivity in the low temperature region,

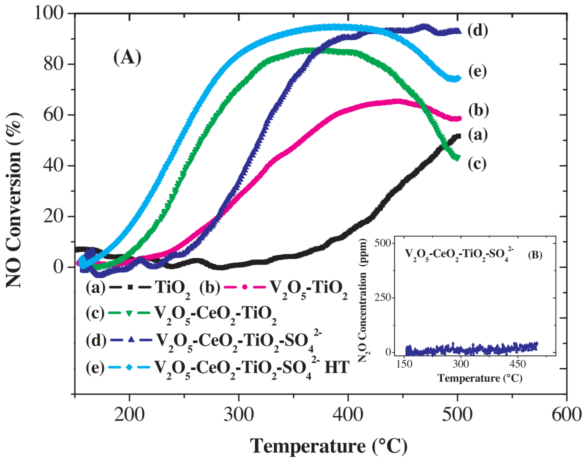

Fig. 9. (A): Reaction temperature dependence of NO conversion over the aerogel catalysts (B): N_2O concentration as a function of SCR reaction temperature over V_2O_5-CeO_2-$TiO_2.SO_4^{2-}$, [NO] = [NH_3] = 0.04%; [O_2] = 8.00% and balance with He, (GHSV) = 120 000 h^{-1}.

whereas the SCR reaction in the high temperature region is likely controlled by the surface acid properties. The importance of the redox property of catalysts in low temperature NH_3-SCR can be also reflected by shifting the reaction pathway from "standard SCR" to "fast SCR".

The curves of the NO-SCR by NH_3 are depicted in Fig. 9A. The TiO_2 support exhibits low NO conversion relating to the presence of only acid sites and the absence of redox ones on the TiO_2 surface. The addition of vanadium without or with cerium increased the NO conversion to N_2 at low temperature, especially in the case of the sample containing Ce. This highlight the potential role of the redox sites created by vanadium (V^{5+}/V^{4+}) and particularly by cerium (Ce^{4+}/Ce^{3+}), on the V_2O_5-TiO_2 and V_2O_5-CeO_2-TiO_2 surface, for the low temperature NH_3-SCR of NO.

At high temperature, NO conversion and N_2 selectivity decrease over V_2O_5-TiO_2 and V_2O_5-CeO_2-TiO_2 catalysts probably due to the secondary reaction of NH_3 oxidation. Conversely, the addition of sulfate enhances both NO conversion and N_2 selectivity at high temperature (> 375 °C) leading to more active and selective V_2O_5-CeO_2-$TiO_2.SO_4^{2-}$ catalyst compared to the sulfate free ones. Noticeably, above 90% NO conversion with a high N_2 selectivity were achieved, in 400–500 °C temperature range, over the sulfated aerogel catalyst (Table 3 and Fig. 9 B) demonstrating the beneficial role of the strong acid sites (probably acting as Brønsted sites) generated by sulfate groups on the V_2O_5-CeO_2-$TiO_2.SO_4^{2-}$ surface for the high temperature SCR-NO by NH_3. According to Z. Si et al. [37], the Brønsted acid sites introduced by sulfate modification, which were less oxidative than Lewis acid sites, weaken the strong oxidation of ammonia but enhance the ammonia adsorption capacity of catalyst and consequently improve its high temperature NO-SCR activity and N_2 selectivity. Nevertheless, it seems that the interactions between sulfate groups and cerium species reduce the number of the active Ce redox sites in the low temperature SCR-NO by NH_3 since the binary V_2O_5-CeO_2-TiO_2 was found more active than the ternary V_2O_5-CeO_2-TiO_2-SO_4^{2-} in 210–360 °C temperature range. Based on the XPS and UV–vis results, this can be correlated with the presence of a low amount of Ce^{4+} active redox sites on the surface of the sulfated catalyst seeing that the interactions between sulfate anions and cerium species contribute to the stabilization of Ce^{3+} form.

Table 3
Catalytic performances of V_2O_5-CeO_2-TiO_2-SO_4^{2-} nanostructured aerogel catalyst calcined at 500 °C in NO-SCR by NH_3: *[NO] = [NH_3] = 0.04%, [O_2] = 8.00% balance with He and (GHSV) = 120 000 h^{-1}.*

Aerogel catalyst	Temperature (°C)	NO Conversion (%)	Selectivity (%)		
			N_2	N_2O	NO_2
V_2O_5-CeO_2-TiO_2-SO_4^{2-}	200	0.3	100	0	0
	250	3.8	100	0	0
	300	34.0	100	0	0
	350	76.4	100	0	0
	400	91.5	99	1	0
	450	92.1	97	3	0
	500	92.1	90	10	0

The hydrothermal treatment significantly improves the low temperature SCR activity of V_2O_5-CeO_2-$TiO_2.SO_4^{2-}$ HT (200–420 °C) but leads to a decrease of NO conversion and N_2 selectivity at high temperature. This could be attributed to *(i)* the loss of the strong acidity (which play an important role in the adsorption and activation of NH_3 at high temperature [88]) and *(ii)* the formation of more Ce^{4+} redox sites (which govern the reactivity of the catalyst at low temperature [88]) and this after sulfate departure during the hydrotreatment of the sample at 625 °C for 16 h.

Noting that, in spite of its very low or even absent acidity, the V_2O_5-CeO_2-TiO_2-SO_4^{2-} HT exhibits high NO reduction to N_2 at low temperature. According to Z. Ma et al. [89,90], the reaction between adsorbed NO_x and gaseous NH_3 seems to be a possible route for the NH_3-SCR process over this catalyst.

Importantly, under the same experimental conditions, the novel V_2O_5-CeO_2-TiO_2-SO_4^{2-} calcined at 500 °C exhibits better catalytic performances in NO-SCR by NH_3, at high temperature (> 450 °C), with respect to V_2O_5-WO_3/TiO_2 EUROCAT commercial catalyst (Fig. 10 A). It demonstrates, after hydrothermal aging at 625 °C for 16 h, approximately a similar catalytic behavior in 200–500 °C temperature range

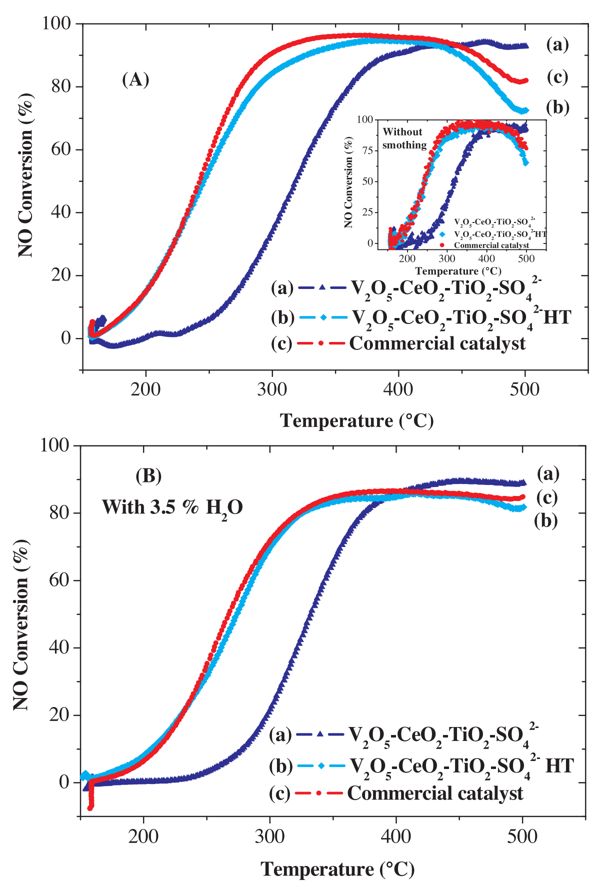

Fig. 10. NO conversion versus reaction temperature over V_2O_5-CeO_2-TiO_2-SO_4^{2-} aerogel catalyst (before and after hydrothermal treatment) and V_2O_5-WO_3/TiO_2 commercial one. [NO] = [NH_3] = 0.04%; [O_2] = 8.00% and balance with He, (GHSV) = 120 000 h^{-1}: (A) without H_2O and (B) with 3.5% H_2O.

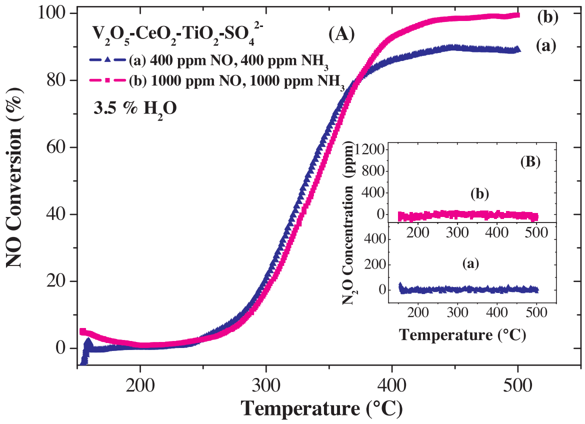

Fig. 11. Effect of NO concentration on the SCR activity of V_2O_5-CeO_2-TiO_2-SO_4^{2-} aerogel catalyst: [NO] = [NH_3] = 0.04% (a) or 0.1% (b); [O_2] = 8.00% and balance with He, 3.5% H_2O, (GHSV) = 120 000 h^{-1}. (A) NO Conversion (%) and (B) N_2O concentration (ppm).

compared to the commercial one. The EUROCAT, which was chosen as a reference catalyst in a joint European project on de-NOx [91,92], is a more complex system than V_2O_5-CeO_2-TiO_2-SO_4^{2-}, containing 3.15 wt% V_2O_5, 9 wt% WO_3, 6.5 wt% SiO_2, 1.5 wt% Al_2O_3, 1 wt% CaO, 0.85 wt% SO_4^{2-} and 78 wt% TiO_2 [93].

The effect of H_2O on the catalytic performances of V_2O_5-CeO_2-TiO_2.SO_4^{2-}, V_2O_5-CeO_2-TiO_2.SO_4^{2-} HT aerogel materials and V_2O_5-WO_3/TiO_2 commercial one was studied and the results are presented in Fig. 10 B. When 3.5% H_2O was added to the reaction gas mixture, a slight decrease of NO conversion is observed indicating a well resistance to water vapor of the solids in 200–500 °C temperature range.

In order to point out the efficiency of the new V_2O_5-CeO_2-TiO_2.SO_4^{2-} aerogel catalyst for NH_3-SCR process in the presence of water (3.5% H_2O), the NO conversion and the N_2O production versus reaction temperature, under two different NO concentrations (400 ppm and 1000 ppm), are illustrated in Fig. 11. The catalytic performances of V_2O_5-CeO_2-TiO_2.SO_4^{2-} aerogel solid in terms of NO conversion, NO_2, N_2O and N_2 selectivity are given in table. 4.

Interestingly, in the presence of 3.5% H_2O, a high SCR activity (NO conversions > 85% with a complete N_2 selectivity) is obtained, in 400–500 °C temperature range, over the V_2O_5-CeO_2-TiO_2.SO_4^{2-} aerogel catalyst calcined at 500 °C. The NO-SCR activity is improved at high temperature by increasing the NO concentration. More interesting, above 99% NO conversion with 100% N_2 selectivity are achieved, in 450–500 °C temperature range, when the NO-SCR reaction was carried out using the concentrations [NO] = [NH_3] = 1000 ppm.

The turnover frequency (TOF, h^{-1}), defined as the number of mole of NO converted per mole of vanadium (and per hour) present in the catalyst, was calculated for all the samples, at three different temperatures (180, 200 and 220 °C), and presented in Fig. 12. The result demonstrates that the TOF values increase by adding cerium, after the hydrothermal aging of V_2O_5-CeO_2-TiO_2.SO_4^{2-} catalyst and by increasing both the reaction temperature and the NO concentration. This confirm the key role of cerium redox sites and the beneficial effect of increasing both the reaction temperature and the NO concentration for $DeNO_x$ing at low temperature.

4. Conclusions and perspectives

This study demonstrates the successful synthesis of a new generation of V_2O_5-TiO_2, V_2O_5-CeO_2-TiO_2 and V_2O_5-CeO_2-TiO_2-SO_4^{2-} nanostructured aerogel catalysts with high surface area, large porosity and good thermal stability. The V_2O_5-TiO_2 derived sol gel catalyst exhibits low NO conversion in (150–500 °C) temperature range with a low N_2 selectivity at high temperature (> 450 °C). The incorporation of cerium increases significantly the NO conversion to N_2 at low temperature leading to a potential V_2O_5-CeO_2-TiO_2 catalyst for $DeNO_x$ing from mobile source in 220–400 °C temperature range. The enhancement of the catalytic performances of V_2O_5-TiO_2 by cerium addition is essentially correlated with the redox sites created by cerium species. The Ce redox sites were found more active than V redox sites and play a major role in SCR-NO by NH_3 at low temperature, under oxygen rich atmosphere. After sulfation of V_2O_5-CeO_2-TiO_2 catalyst, the maximum NO conversion was shifted toward high temperature indicating a modification in the reactivity of Ce redox sites due to their interactions with sulfates groups. Over V_2O_5-CeO_2-TiO_2-SO_4^{2-} catalyst calcined at 500 °C, NO conversion and N_2 selectivity remain important in 380–500 °C temperature range underlying the potential role of the strong acid sites created by sulfates groups for the high temperature NO-SCR by NH_3.

The novel V_2O_5-CeO_2-TiO_2-SO_4^{2-} nanostructured aerogel catalyst calcined at 500 °C exhibits better NH_3-SCR catalytic performances, in 450 °C–500 °C, compared to V_2O_5-WO_3/TiO_2 EUROCAT. It keeps its efficiency in presence of water vapor and its catalytic performances are improved by increasing the NO concentration during the SCR reaction. Interstingly, more than 99% NO conversion with 100% N_2 selectivity was achieved, in 450–500 °C temperature range over V_2O_5-CeO_2-TiO_2-SO_4^{2-} aerogel catalyst calcined at 500 °C, when the NO-SCR reaction was realized using the concentrations [NO] = [NH_3] = 1000 ppm, in the presence of 3.5% H_2O.

Table 4
Catalytic performances of V_2O_5-CeO_2-TiO_2-SO_4^{2-} nanostructured aerogel catalyst calcined at 500 °C in NH_3-SCR of NO with 3.5% H_2O under different NO concentrations.

Aerogel catalyst and catalytic conditions	Temperature (°C)	NO Conversion (%)	Selectivity (%)		
			N_2	N_2O	NO_2
V_2O_5-CeO_2-TiO_2-SO_4^{2-}	200	0.0	100	0	0
[NO] = [NH_3] = 0.04%	250	2.4	100	0	0
[O_2] = 8.00% balance with He	300	20.4	100	0	0
(GHSV) = 120 000 h^{-1}	350	65.8	100	0	0
3.5% H_2O	400	86.5	100	0	0
	450	89.8	100	0	0
	500	88.3	100	0	0
V_2O_5-CeO_2-TiO_2-SO_4^{2-}	200	0.3	100	0	0
[NO] = [NH_3] = 0.1%	250	2.7	100	0	0
[O_2] = 8.00% balance with He	300	18.5	100	0	0
(GHSV) = 120 000 h^{-1}	350	58.8	100	0	0
3.5% H_2O	400	94.2	100	0	0
	450	99.1	100	0	0
	500	99.1	100	0	0

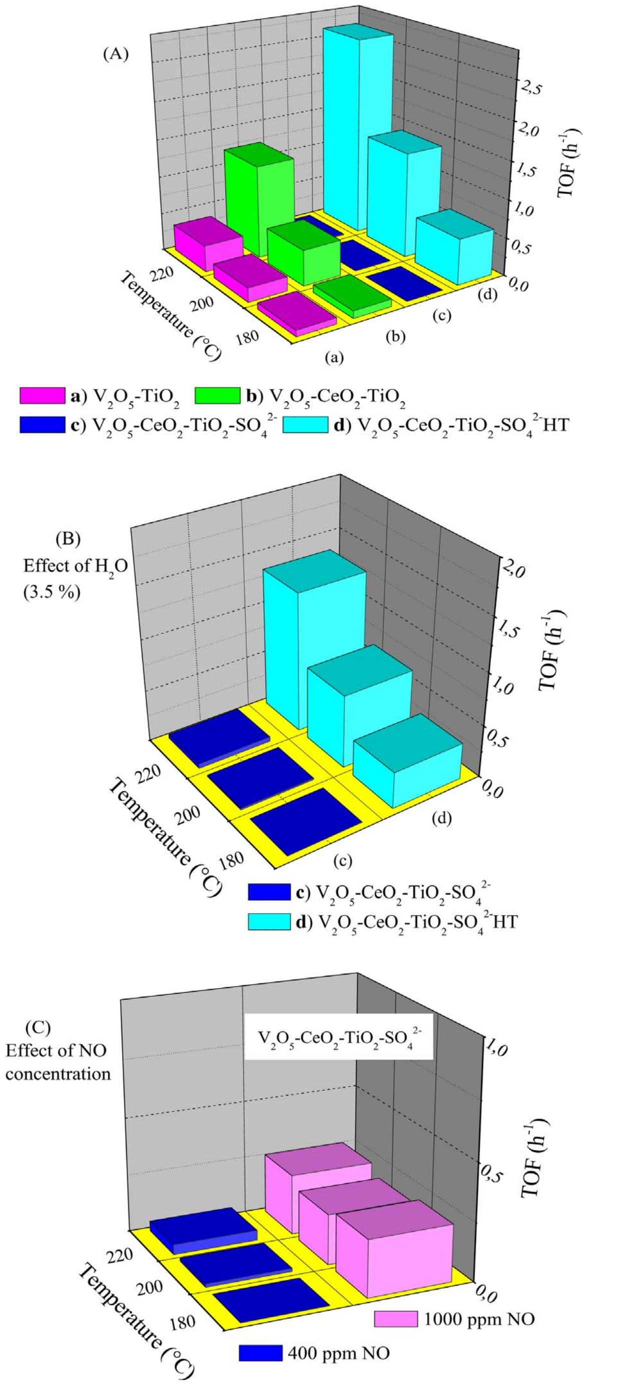

Fig. 12. TOF values, defined at 180, 200 and 220 °C, over the nanostructured aerogel catalysts: (A) [NO] = [NH_3] = 0.04% without H_2O; (B) Effect of H_2O (3.5%); (C) Effect of NO concentration with 3.5% H_2O.

Further studies are in progress to investigate more extensively the hydrothermal stability of the novel V_2O_5-CeO_2-TiO_2-$SO_4{}^{2-}$ aerogel material, to evaluate the effect of SO_2 in the SCR activity and to understand the NH_3-SCR mechanism over these novel catalysts at different reaction temperatures. It is also necessary to extend the windows of temperature for V_2O_5-CeO_2-TiO_2-$SO_4{}^{2-}$ at low temperatures, while improve the activity for V_2O_5-CeO_2-TiO_2-$SO_4{}^{2-}$ HT at high temperatures.

Acknowledgements

The authors wish to express their sincere thanks to Thomas Cacciaguerra, Valérie Flaud and Prof. Mehrez Oueslati for XRD, XPS and Raman analysis, respectively. Financial support by Laboratory of Chemistry of Materials and Catalysis (LCMC) of Tunisia and Franco-Tunisian Cooperation (French Institute of Tunisia, SSHN grant) are gratefully acknowledged.

References

[1] H. Bosch, F. Janssen, Catalytic reduction of nitrogen oxides. A review on the fundamentals and technology, Catal. Today 2 (1988) 369–521.
[2] G.S. Qi, R.T. Yang, Low-temperature selective catalytic reduction of NO with NH_3 over iron and manganese oxides supported on titania, Appl. Catal. B: Environ. 44 (2003) 217–225.
[3] H. Phil, M. Reddy, P. Kumar, L. Ju, J. Hyo, SO_2 resistant antimony promoted V_2O_5/TiO_2 catalyst for NH_3-SCR of NO_x at low temperatures, Appl. Catal. B: Environ. 78 (2008) 301–308.
[4] Z.F. Lu, D.G. Streets, Increase in NO_x emissions from Indian thermal power plants during 1996–2010: Unit-Based Inventories and multisatellite observations, Environ. Sci. Technol. 46 (2012) 7463–7470.
[5] N.Y. Topsøe, Mechanism of the selective catalytic reduction of nitric oxide by ammonia elucidated by in situ on-line Fourier transform infrared spectroscopy, Science (1994) 1217–1219 Washington, /265.
[6] M. Koebel, M. Elsener, T. Marti, NO_x-Reduction in diesel exhaust gas with urea and selective catalytic reduction, Combust. Sci. Technol. 121 (1996) 85–102.
[7] S. Roy, M.S. Hegde, G. Madras, Catalysis for NO_x abatement, Appl. Energy 86 (2009) 2283–2297.
[8] P. Granger, V.I. Parvulescu, Catalytic NO_x abatement systems for mobile sources: from three-Way to lean burn after-treatment technologies, Chem. Rev. 111 (2011) 3155–3207.
[9] D. Worch, W. Suprun, R. Gläser, Supported transition metal-oxide catalysts for HC-SCR $DeNO_x$ with propene, Catal. Today 176 (2011) 309–313.
[10] A.N. Mendes, V.L. Zholobenko, F.T. Starzyk, P.D. Costa, C. Henriques, On the enhancing effect of Ce in Pd-MOR catalysts for NO_x CH_4-SCR: A structure-reactivity study, Appl. Catal. B: Environ. 195 (2016) 121–131.
[11] Z. Li, J. Li, S. Liu, X. Ren, J. Ma, W. Su, Y. Peng, Ultra hydrothermal stability of CeO_2-WO_3/TiO_2 for NH_3-SCR of NO compared to traditional V_2O_5-WO_3/TiO_2 catalyst, Catal. Today 258 (2015) 11–16.
[12] G. Busca, L. Lietti, G. Ramis, F. Berti, Chemical and mechanistic aspects of the selective catalytic reduction of NOx by ammonia over oxide catalysts: a review, Appl. Catal. B: Environ. 18 (1998) 1–36.
[13] S. Brandenberger, O. Kröcher, A. Tissler, R. Althoff, The state of the art in selective catalytic reduction of NO_x by ammonia using metal-exchanged zeolite catalysts, Catal. Rev. Sci. Eng. 50 (2008) 492–531.
[14] F. Liu, Y. Yu, H. He, Environmentally-benign catalysts for the selective catalytic reduction of NO_x from diesel engines: structure–activity relationship and reaction mechanism aspects, Chem. Commun. 50 (2014) 8445–8463.
[15] W. Shan, F. Liu, H. He, X. Shi, C. Zhang, A superior Ce-W-Ti mixed oxide catalyst for the selective catalytic reduction of NO_x with NH_3, Appl. Catal. B: Environ. 115–116 (2012) 100–106.
[16] I. Nova, D. Bounechada, R. Maestri, E. Tronconi, Influence of the substrate properties on the performances of NH_3-SCR monolithic catalysts for the after treatment of diesel exhaust: an experimental and modeling study, Ind. Eng. Chem. Res. 50 (2011) 299–309.
[17] C. Tang, H. Zhang, L. Dong, Ceria-based catalysts for low-temperature selective catalytic reduction of NO with NH_3, Catal. Sci. Technol. 6 (2016) 1248–1264.
[18] L. Chen, Z. Si, X. Wu, D. Weng, R. Ran, J. Yu, Rare earth containing catalysts for selective catalytic reduction of NO_x with ammonia: a review, J. Rare Earth 32 (2014) 907–917.
[19] A. Trovarelli, M. Boaro, E. Rocchini, G. Dolcetti, Some recent developments in the characterization of ceria-based catalysts, J. Alloys Comp. 323–324 (2001) 584–591.
[20] B.M. Reddy, A. Khan, Y. Yamada, T. Kobayashi, S. Loridant, J.C. Volta, Structural characterization of CeO_2-TiO_2 and V_2O_5/CeO_2-TiO_2 catalysts by Raman and XPS techniques, J. Phys. Chem. B 107 (2003) 5162–5167.
[21] X. Gao, Y. Jiang, Y. Zhong, Z.Y. Luo, K. Cen, The activity and characterization of CeO_2-TiO_2 catalysts prepared by the sol-gel method for selective catalytic reduction of NO with NH_3, J. Hazard. Mater. 174 (2010) 734–739.
[22] L. Matějová, K. Kočí, M. Reli, L. Čapek, A. Hospodková, P. Peikertová, Z. Matěj, L. Obalová, A. Wach, P. Kuśtrowski, A. Kotarba, Preparation, characterization and photocatalytic properties of cerium doped TiO_2: On the effect of Ce loading on the photocatalytic reduction of carbon dioxide, Appl. Catal. B: Environ. 152–153 (2014) 172–183.
[23] M.J. Muñoz-Batista, M. Milagros Ballari, A. Kubacka, A.E. Cassano, O.M. Alfano, M. Fernández-García, Acetaldehyde degradation under UV and visible irradiation using CeO_2-TiO_2 composite systems: evaluation of the photocatalytic efficiencies, Chem. Eng. J. 255 (2014) 297–306.
[24] C. Gannoun, R. Delaigle, P. Eloy, D.P. Debecker, A. Ghorbel, E.M. Gaigneaux, Effect of support on V_2O_5 catalytic activity in chlorobenzene oxidation, Appl.Catal. A: Gen. 447–448 (2012) 1–6.
[25] H.J. Sedjame, C. Fontaine, G. Lafaye, J. Barbier Jr., On the promoting effect of the addition of ceria to platinum based alumina catalysts for VOCs oxidation, Appl. Catal. B: Environ. 144 (2014) 233–242.
[26] O.A. González Vargas, J.A. De Los Reyes Heredia, A. Montesinos Castellanos, L.F. Chen, J.A. Wang, Cerium incorporating into MCM-41 mesoporous materials for

CO oxidation, Mater. Chem. Phys. 139 (2013) 125–133.

[27] J.L. Ayastuy, A. Iglesias-González, M.A. Gutiérrez-Ortiz, Synthesis and characterization of low amount tin-doped ceria ($Ce_xSn_{1-x}O_{2-\delta}$) for catalytic CO oxidation, Chem. Eng. J. 244 (2014) 372–381.

[28] R.Q. Long, R.T. Yang, The promoting role of rare earth oxides on Fe-exchanged TiO_2-pillared clay for selective catalytic reduction of nitric oxide by ammonia, Appl. Catal. B: Environ. 27 (2000) 87–95.

[29] W.Q. Xu, Y.B. Yu, C.B. Zhang, H. He, Selective catalytic reduction of NO by NH_3 over a Ce/TiO_2 catalyst, Catal. Commun. 9 (2008) 1453–1457.

[30] L. Chen, J. Li, M. Ge, R. Zhu, Enhanced activity of tungsten modified CeO_2/TiO_2 for selective catalytic reduction of NO_x with ammonia, Catal. Today 153 (2010) 77–83.

[31] Y. Huang, Z. Tong, B. Wu, J. Zhang, Low temperature selective catalytic reduction of NO by ammonia over V_2O_5-CeO_2/TiO_2, J. Fuel Chem. Technol. 36 (2008) 616–620.

[32] Q. Li, X. Hou, H. Yang, Z. Ma, J. Zheng, F. Liu, X. Zhang, Z. Yuan, Promotional effect of CeO_x for NO reduction over V_2O_5/TiO_2-carbon nanotube composites, J. Mol. Catal. A 356 (2012) 121–127.

[33] M.S. Maqbool, A.K. Pullur, H. Phil Ha, Novel sulfation effect on low-temperature activity enhancement of CeO_2-added Sb-V_2O_5/TiO_2 catalyst for NH_3-SCR, Appl. Catal. B: Environ. 152–153 (2014) 28–37.

[34] W. Zhao, Q. Zhong, Y.X. Pan, Systematic effects of S-doping on the activity of V_2O_5/TiO_2 catalyst for low-temperature NH_3-SCR, Chem. Eng. J. 228 (2013) 815–823.

[35] J.P. Chen, R.T. Yang, Selective catalytic reduction of NO with NH_3 on SO_4^{2-}/TiO_2 superacid catalyst, J. Catal. 139 (1993) 277–288.

[36] R. Khodayari, C.U. Ingemar Odenbrand, Regeneration of commercial SCR catalysts by washing and sulphation: effect of sulphate groups on the activity, Appl. Catal. B: Environ. 33 (2001) 277–291.

[37] Z. Si, D. Weng, X. Wu, Y. Jiang, Roles of Lewis and Brønsted acid sites in NO reduction with ammonia on CeO_2-ZrO_2-NiO-SO_4^{2-} catalyst, J. Rare Earth. 28 (2010) 727–731.

[38] Y. Jiang, Z. Xing, X. Wang, S. Huang, X. Wang, Q. Liu, Activity and characterization of a Ce-W-Ti oxide catalyst prepared by a single step sol-gel method for selective catalytic reduction of NO with NH_3, Fuel 151 (2015) 124–129.

[39] C. Gannoun, R. Delaigle, P. Eloy, D.P. Debecker, A. Ghorbel, E.M. Gaigneaux, Sol-gel derived V_2O_5-TiO_2 mesoporous materials as catalysts for the total oxidation of chlorobenzene, Catal. Comm. 15 (2011) 1–5.

[40] A. Marberger, M. Elsener, D. Ferri, O. Kröcher, VO_x surface coverage optimization of V_2O_5/WO_3-TiO_2 SCR catalysts by variation of the V loading and by aging, Catalysts 5 (2015) 1704–1720.

[41] K. Cheng, J. Liu, T. Zhang, J. Li, Z. Zhao, Y. Wei, G. Jiang, A. Duan, Effect of Ce doping of TiO_2 support on NH_3-SCR activity over V_2O_5-WO_3/CeO_2-TiO_2 catalyst, J. Environ. Sci. 26 (2014) 2106–2113.

[42] Degussa Tech. Bull. Pigm. Rep. 56 (1990) 13.

[43] J. Arfaoui, L.K. Boudali, A. Ghorbel, G. Delahay, Influence of the nature of titanium source and of vanadia content on the properties of titanium-pillared montmorillonite, J. Phys. Chem. Sol. 69 (2008) 1121–1124.

[44] Z. Si, D. Weng, X. Wu, Z. Ma, J. Ma, R. Ran, Lattice oxygen mobility and acidity improvements of NiO-CeO_2-ZrO_2 catalyst by sulfation for NO_x reduction by ammonia, Catal. Today 201 (2013) 122–130.

[45] J. Arfaoui, A. Ghorbel, C. Petitto, G. Delahay, Novel vanadium supported onto mixed molybdenum-titanium pillared clay catalysts for the low temperature SCR-NO by NH_3, Chem. Eng. J. (2017), http://dx.doi.org/10.1016/j.cej.2017.02.046 in press.

[46] IUPAC, Reporting physisorption data for gas/solid systems with special reference to the determination of surface area and porosity, Pure Appl. Chem. 57 (1985) 603–619.

[47] T. Lopez, F. Rojas, R.A. Katz, F. Galindo, A. Balankin, A. Buljanc, Porosity, structural and fractal study of sol-gel TiO_2-CeO_2 mixed oxides, J. Solid. State Chem. 177 (2004) 1873–1885.

[48] S. Chin, E. Park, M. Kim, G.N. Bae, J. Jurng, Synthesis and photocatalytic activity of TiO_2 nanoparticles prepared by chemical vapor condensation method with different precursor concentration and residence time, J. Colloid Inter. Sci. 362 (2011) 470–476.

[49] B. Guan, H. Lin, L. Zhu, Z. Huang, Selective catalytic reduction of NO_x with NH_3 over Mn Ce substitution $Ti_{0.9}V_{0.1}O_{2-\delta}$ nanocomposites catalysts prepared by self-propagating high-temperature synthesis method, J. Phys. Chem. C 115 (2011) 12850–12863.

[50] S. Gillot, J.P. Dacquin, C. Dujardin, P. Granger, High Intrinsic Catalytic Activity of $CeVO_4$-Based Catalysts for Ammonia-SCR: Influence of pH During Hydrothermal Synthesis, Top. Catal. 59 (2016) 987–995.

[51] N. Wetchakun, B. Incessungvorn, K. Wetchakun, S. Phanichphant, Influence of calcination temperature on anatase to rutile phase transformation in TiO_2 nanoparticles synthesized by the modified sol-gel method, Mater. Lett. 82 (2012) 195–198.

[52] Z. Ma, X. Wu, Y. Feng, Z. Si, D. Weng, L. Shi, Low-temperature SCR activity and SO_2 deactivation mechanism of Ce-modified V_2O_5-WO_3/TiO_2 catalyst, Prog. Nat. Sci. 25 (2015) 342–352.

[53] Choo, Y.G. Lee, I.S. Nam, S.W. Ham, J.B. Lee, Characteristics of V_2O_5 supported on sulfated TiO_2 for selective catalytic reduction of NO by NH_3, Appl. Catal. A Gen. 200 (2000) 177–188.

[54] X. Gu, J. Ge, H. Zhang, A. Auroux, J. Shen, Structural, redox and acid?base properties of V_2O_5/CeO_2 catalysts, Thermochim. Acta 451 (2006) 84–93.

[55] Z. Liu, S. Zhang, J. Li, J. Zhu, L. Ma, Novel V_2O_5-CeO_2/TiO_2 catalyst with low vanadium loading for the selective catalytic reduction of NOx by NH_3, Appl. Catal. B: Environ. 158–159 (2014) 11–19.

[56] S.M. Lee, S.C. Hong, Promotional effect of vanadium on the selective catalytic oxidation of NH_3 to N_2 over Ce/V/TiO $_2$ catalyst, Appl. Catal. B: Environ. 163 (2015) 30–39.

[57] D. Pang, L. Qiu, R. Zhu, F. Ouyang, Silica supported SO_4^{2-}/TiO_2 for photocatalytic decomposition of acrylonitrile under simulant solar light irradiation, Chem. Eng. J. 270 (2015) 590–596.

[58] X.C. Wang, J.C. Yu, P. Liu, X.X. Wang, W.Y. Su, X.Z. Fu, Probing of photocatalytic surface sites on SO_4^{2-}/TiO_2 solid acids by in situ FT-IR spectroscopy and pyridine adsorption, J. Photochem. Photobiol. A 179 (2006) 339–347.

[59] W. Shan, F. Liu, H. He, X. Shi, C. Zhang, A superior Ce-W-Ti mixed oxide catalyst for the selective catalytic reduction of NO_x with NH_3, Appl. Catal. B: Environ. 115–116 (2012) 100–106.

[60] W. Shan, F. Liu, H. He, X. Shi, C. Zhang, An environmentally-benign CeO_2-TiO_2 catalyst for the selective catalytic reduction of NOx with NH_3 in simulated diesel exhaust, Catal. Today 184 (2012) 160–165.

[61] S. Gao, X. Chen, H. Wang, J. Mo, Z. Wu, Y. Liu, X. Weng, Ceria supported on sulfated zirconia as a superacid catalyst for selective catalytic reduction of NO with NH_3, J. Colloid Inter. Sci. 394 (2013) 515–521.

[62] X.S. Du, X. Gao, L.W. Cui, Y.C. Fu, Z.Y. Luo, K.F. Cen, Investigation of the effect of Cu addition on the SO_2 resistance of a Ce-Ti oxide catalyst for selective catalytic reduction of NO with NH_3, Fuel 92 (2012) 49–55.

[63] L. Baraket, A. Ghorbel, P. Grange, Selective catalytic reduction of NO by ammonia on V_2O_5-SO_4^{2-}/TiO_2 catalysts prepared by the sol-gel method, Appl. Catal. B: Environ. 72 (2007) 37–43.

[64] H. Zhao, S. Bennici, J. Shen, A. Auroux, The influence of the preparation method on the structural, acidic and redox properties of V_2O_5-TiO_2/SO_4^{2-}catalysts, Appl. Catal. A: Gen. 356 (2009) 121–128.

[65] Y. Segura, L. Chmielarz, P. Kustrowski, P. Cool, R. Dziembaj, E.F. Vansant, Characterisation and reactivity of vanadia–titania supported SBA-15 in the SCR of NO with ammonia, Appl. Catal. B: Environ. 61 (2005) 69–78.

[66] J. Arfaoui, L.K. Boudali, A. Ghorbel, G. Delahay, Effect of vanadium on the behaviour of unsulfated and sulfated Ti-pillared clay catalysts in the SCR of NO by NH_3, Catal. Today 142 (2009) 234–238.

[67] M. Morey, A. Davidson, H. Eckert, G. Stucky, Pseudotetrahedral $O_{3/2}V = O$ centers immobilized on the walls of a mesoporous, cubic MCM-48 support: preparation, characterization, and reactivity toward water As investigated by ^{51}V NMR and UV–vis spectroscopies, Chem. Mater. 8 (1996) 486–492.

[68] M. Baltes, K. Cassiers, P. Van Der Voort, B.M. Weckhuysen, R.A. Schoonheydt, E.F. Vansant, MCM-48-supported vanadium oxide catalysts, prepared by the molecular designed dispersion of $VO(acac)_2$: a detailed study of the highly reactive MCM-48 surface and the structure and activity of the deposited VOx, J. Catal. 197 (2001) 160–171.

[69] A. Held, P. Florczak, Vanadium, niobium and tantalum modified mesoporous molecular sieves as catalysts for propene epoxidation, Catal. Today 142 (2009) 329–334.

[70] V. Murgia, E.M.F. Torres, J.C. Gottifredi, E.L. Sham, Sol–gel synthesis of V_2O_5-SiO_2 catalyst in the oxidative dehydrogenation of n-butane, Appl. Catal. A: Gen. 312 (2006) 134–143.

[71] W.J. Roth, B. Gil, W. Makowski, A. Sławek, A. Korzeniowska, J. Grzybek, M. Siwek, P. Michorczyk, Framework-substituted cerium MCM-22 zeolite and its interlayer expanded derivative MWW-IEZ, Catal. Sci. Technol. (2016), http://dx.doi.org/10.1039/c5cy02074c.

[72] Y. Wu, J. Wang, P. Liu, W. Zhang, J. Gu, X. Wang, Framework-substituted lanthanide MCM-22 zeolite: synthesis and characterization, J. Am. Cem. Soc. 132 (2010) 17989–17991.

[73] Y. Shao, L. Wang, J. Zhang, M. Anpo, Synthesis of hydrothermally stable and long-range ordered Ce-MCM-48 and Fe-MCM-48 materials, J. Phys. Chem. B 109 (2005) 20835–20841.

[74] D.E. Keller, T. Visser, F. Soulimani, D.C. Koningsberger, B.M. Weckhuysen, Hydration effects on the molecular structure of silica-supported vanadium oxide catalysts: a combined IR, Raman, UV–vis and EXAFS study, Vib. Spectrosc. 43 (2007) 140–151.

[75] K.V. Bineesh, D.K. Kim, M.I. Kim, D.W. Park, Selective catalytic oxidation of H_2S over V_2O_5 supported on TiO_2-pillared clay catalysts in the presence of water and ammonia, Appl. Clay Sci. 53 (2011) 204–211.

[76] J. Arfaoui, L.K. Boudali, A. Ghorbel, G. Delahay, Characterization and catalytic performance of vanadium supported on sulfated Ti-PILC catalysts issued from different Ti-precursors in selective catalytic reduction of nitrogen oxide by ammonia, J. Mater. Sci. 44 (2009) 6670–6676.

[77] H. Zhao, S. Bennici, J. Cai, J. Shen, A. Auroux, Influence of the metal oxide support on the surface and catalytic properties of sulfated vanadia catalysts for selective oxidation of methanol, J. Catal. 274 (2010) 259–272.

[78] J. Arfaoui, L.K. Boudali, A. Ghorbel, G. Delahay, Vanadium supported on sulfated Ti-pillared clay catalysts: effect of the amount of vanadium on SCR-NO by NH_3 activity, Stud. Surf. Sci. Catal. 174 (2008) 1263–1266.

[79] F. Arena, R. Dario, A. Parmaliana, A characterization study of the surface acidity of solid catalysts by temperature programmed methods, Appl. Catal. A: Gen. 170 (1998) 127–137.

[80] S.M. Jung, P. Grange, The investigation of mechanism of SCR reaction on a TiO_2-SO_4^{2-} catalyst by DRIFTS, Appl. Catal. B: Environ 27 (2000) 11–16.

[81] J. Arfaoui, L.K. Boudali, A. Ghorbel, Catalytic epoxidation of allylic alcohol (E)-2-hexen-1-ol over vanadium supported on unsulfated and sulfated titanium pillared montmorillonite catalysts: effect of sulfate groups and vanadium loading, Appl. Clay Sci. 48 (2010) 171–178.

[82] Q. Zhang, J. Zhang, Z. Song, P. Ning, H. Li, X. Liu, A novel and environmentally friendly SO_4^{2-}/CeO_2 catalyst for the selective catalytic reduction of NO with NH_3, J. Ind. Eng. Chem. 34 (2016) 165–171.

[83] Z. Si, D. Weng, X. Wu, J. Yang, B. Wang, Modifications of CeO_2-ZrO_2 solid solutions by nickel and sulfate as catalysts for NO reduction with ammonia in excess O_2, Catal. Comm. 11 (2010) 1045–1048.
[84] X. Guo, C. Bartholomew, W. Hecker, L.L. Baxter, Effects of sulfate species on V_2O_5/TiO_2 SCR catalysts in coal and biomass-fired systems, Appl. Catal. B: Environ. 92 (2009) 30–40.
[85] L. Jun-Cheng, X. Lan, X. Feng, W. Zhan-Wen, W. Fei, Effect of hydrothermal treatment on the acidity distribution of γ-Al_2O_3 support, Appl. Surf. Sci. 253 (2006) 766–770.
[86] L. Ma, Y. Cheng, G. Cavataio, R.W. McCabe, L. Fu, J. Li, Characterization of commercial Cu-SSZ-13 and Cu-SAPO-34 catalysts with hydrothermal treatment for NH_3-SCR of NO_x in diesel exhaust, Chem. Eng. J. 225 (2013) 323–330.
[87] T. Grzybek, Layered clays as SCR deNOx catalysts, Catal. Today 119 (2007) 125–132.
[88] L. Lietti, J.L. Alemany, P. Forzatti, G. Busca, G. Ramis, E. Giamello, F. Bregani, Reactivity of V_2O_5-WO_3/TiO_2 catalysts in the selective catalytic reduction of nitric oxide by ammonia, Catal. Today 29 (1996) 143–148.
[89] Z. Ma, H. Yang, B. Li, F. Liu, X. Zhang, Temperature-dependent effects of SO_2 on selective catalytic reduction of NO over Fe-Cu-O_x/CNTs-TiO_2 catalysts, Ind. Eng. Chem. Res. 52 (2013) 3708–3713.
[90] Z. Ma, H. Yang, F. Liu, X. Zhang, State Interaction between SO_2 and Fe-Cu-O_x/CNTs-TiO_2 catalyst and its influence on NO reduction with NH_3, Appl. Catal. A: General 467 (2013) 450–455.
[91] Special issue on EUROCAT deNOx SCR project, Catal. Today 56 (4) (2000).
[92] A.F. Popa, P.H. Mutin, A. Vioux, G. Delahay, B. Coq, Novel non-hydrolytic synthesis of a V_2O_5-TiO_2 xerogel for the selective catalytic reduction of NOx by ammonia, Chem. Commun. 221 (2004) 2214–2215.
[93] J.C. Védrine, Industrial features, Catal. Today 56 (2000) 333–334.